JOURNAL OF MATERIALS SCIENCE 31 (1996) 3513–3521

Fractal dimension of the grain boundary fracture in creep–fracture of cobalt-based heat resistant alloys

MANABU TANAKA
Department of Mechanical Engineering Mining College, Akita University 1-1, Tegatagakuen-cho, Akita 010, Japan

The effects of grain boundary configuration and creep conditions on the fractal dimension of the grain boundary fracture (D_f) were investigated using commercial cobalt-based heat resistant alloys, namely, HS–21 and L–605 alloys. Creep-rupture experiments were carried out under the initial creep stresses of 19.6–176 MPa in the temperature range from 1089–1422 K in air. The value of D_f was larger in specimens with serrated grain boundaries than in those with straight grain boundaries in the HS–21 alloy under the same creep condition, and the difference in the value of D_f between these specimens was large in the scale range of the analysis which was less than about one grain boundary length. However, there was almost no difference in the value of D_f between the specimens with serrated grain boundaries and those with straight grain boundaries in the L–605 alloy, because there was no obvious difference in the microstructure between these specimens. The value of D_f increased with decreasing creep stress in the scale range of the fractal analysis larger than about one grain boundary length in both HS–21 and L–605 alloys, while the stress dependence of D_f was larger in the HS–21 alloy. The stress dependence of D_f was explained by the stress dependence on the number of grain boundary microcracks linked to the fracture surface. The value of D_f estimated in the scale range smaller than about one grain boundary length showed essentially no stress dependence in both L–605 and HS–21 alloys.

1. Introduction

The concept of fractal geometry has been applied to the analysis of problems and the interpretation of phenomena in applied mathematics, physics, chemistry and materials science [1]. In the sphere of materials science, Mandelbrot *et al.* [2] first revealed that for impact-loaded and fractured steels, the absorbed energy decreased with increasing fractal dimension of the fracture surface. Banerji and Underwood [3, 4] reported that embrittlement of tempered 4340 steel can be related to the minimum value of the fractal dimension of fracture surface profiles. Microstructures in metallic materials often have a fractal nature and can be characterized by the fractal dimension [5, 6] Dauskardt *et al.* [7] also reported on the correlation between the fractal dimension of fracture surface profiles and microstructures of materials.

It has been revealed that for several heat resistant alloys there is a correlation between the improvement in creep–rupture properties and the relative increase of the fractal dimension of the grain boundaries (the fractal dimension of the grain boundary profiles in the two-dimensional section (D_{gb}, $1 < D_{gb} < 2$) by heat treatments [8]. There is also a correlation between the fractal dimension of the grain boundary fracture surface profile in the longitudinal section (D_f, $1 < D_f < 2$) (the fractal dimension of the grain boundary fracture), the creep–rupture properties and the fracture mechanisms in these alloys [9]. Grain boundary fracture patterns were affected not only by microstructures such as grain boundary configuration and grain size but also by creep conditions [10, 11].

In this study, creep–rupture experiments were carried out using commercial cobalt-based heat resistant alloys, namely, HS–21 and L–605 alloys under initial creep stresses of 19.6–176 MPa in the temperature range from 1089–1422 K in air. Creep conditions were chosen to cause grain boundary fracture in all the specimens of the cobalt-based alloys in this study. The effects of grain boundary configuration and creep conditions on the fractal dimension of the grain boundary fracture (D_f) were examined on the ruptured specimens of these alloys. The value of D_f was estimated in both scale ranges of the fractal analysis, namely smaller than or larger than about one grain boundary length of the specimens. As in a previous studies [10, 11], the vertical section method,

0022–2461

in which the grain boundary microcracks linked to the fracture surface were taken into account, was utilized in order to examine the value of D_f.

2. Experimental procedure

Table I shows the chemical composition of the two cobalt-based heat resistant alloys used in this study. As reported in the previous studies [10, 11], these alloys were heat-treated to generate serrated or straight grain boundaries whilst keeping the matrix strength and grain size almost the same in each alloy. The fractal dimension of the grain boundary profiles in the two-dimensional section (D_{gb}, $1 < D_{gb} < 2$), or shortly, the fractal dimension of the grain boundaries was determined by the box-counting method [1, 12, 13]. Table II shows the heat-treatments, the fractal dimension of the grain boundaries (D_{gb}) and the grain diameter (d_g) of the specimens in the cobalt-based superalloys. The values of D_{gb} and d_g were cited from a previous study [8]. In this study, the types of grain boundaries were conventionally classified into two categories, namely, "serrated grain boundaries" and "straight grain boundaries" according to the relative magnitude of D_{gb}, although there is only a little difference in the value of D_{gb} between them in the L–605 alloy (Table II). The heat-treated specimens were machined into creep–rupture test pieces of 5 or 6 mm diameter and 30 mm gauge length. Creep–rupture experiments were carried out using these test pieces with creep–rupture equipment of the single-lever type under initial creep stresses (constant load test conditions) in the range from 19.6–176 MPa at temperatures from 1089–1422 K in air. All the test pieces were held for 10.8 ks at each test temperature before loading.

The fractal dimension of the grain boundary fracture surface profile (D_f, $1 < D_f < 2$), or shortly, the fractal dimension of the grain boundary fracture in the ruptured specimens was estimated by the vertical section method [14, 15]. The ruptured specimens were longitudinally sectioned in the plane involving the vertical axis and the fracture surface profiles were examined using both optical and scanning electron microscopes at various magnifications up to 10000 times. As in previous studies [10, 11], the box-counting method [1, 12, 13] was employed to determine the value of D_f.

Fig. 1 shows a schematic illustration of the box-counting method applied to the estimation of D_f in the scale ranges (r) both smaller than and larger than about one grain boundary length. The optical micrographs taken on the whole fracture surface profile at a magnification of 50 times were used for the estimation of D_f in the scale range for the analysis (r) larger than about one grain boundary length ($0.68 \leqslant r/d_g \leqslant 34$ for the HS–21 alloy and $0.42 \leqslant r/d_g \leqslant 17$ for the L–605 alloy, where d_g is the grain diameter) (Fig. 1a). The grain boundary microcracks linked to the fracture surface were taken into account in both scale ranges used in this study (Fig. (a, b)). The fracture surface profile of five to eight grain boundary lengths involving at least one grain boundary microcrack was examined on each specimen in order to estimate the value of D_f in the scale range of the analysis smaller than about one grain boundary length ($2.2 \times 10^{-3} \leqslant r/d_g \leqslant 0.65$ for the HS–21 alloy and $1.1 \times 10^{-3} \leqslant r/d_g \leqslant 0.32$ for the L–605 alloy) (Fig. 1b). However, a preliminary study revealed that the value of the fractal dimension estimated in the scale range smaller than about one grain boundary length was almost unchanged by excluding these microcracks in the fractal analysis.

If there is a relationship between the number of square boxes, n, intersecting the fracture surface or involving the grain boundary microcracks linked to the fracture surface (Fig. 1) and the scale length of the fractal analysis (the side length of a box), r, to be expressed through the fractal dimension, D_f, as [1, 5, 6, 8, 12, 13]:

$$n = n_0 r^{-D_f} \tag{1}$$

the length of the fracture surface profile, L, is then given by a product of the side length (r) and the number of the square boxes (n), such that [1, 3–7, 10, 14, 15]:

$$L = r \times n = L_0 r^{1-D_f} \tag{2}$$

TABLE I Chemical composition of the cobalt-based heat resistant alloys used (wt %).

Alloys	C	B	Cr	Ni	Fe	Mn	W	Mo	Si	S	P
HS–21	0.27	0.003	26.71	2.37	0.09	0.64	–	5.42	0.59	0.007	<0.005
L–605	0.07	–	19.82	9.83	2.22	1.46	14.37	–	0.19	0.002	<0.005

Co: bal.

TABLE II The heat treatments, the fractal dimension of the grain boundaries (D_{gb}) (grain boundary configuration) and the grain diameter (d_g) in the specimens of the cobalt-based alloys.

Alloys	Heat treatments	Fractal dimension of the grain boundaries, D_{gb} (grain boundary configuration)	Grain diameter, d_g (μm)
HS–21	1523 K – 3.6 ks – F. C. → 1323 K → W.Q.	1.324 (serrated)	130
	1523 K – 3.6 ks → W.Q.	1.086 (straight)	130
L–605	1473 K – 3.6 ks – F. C. → 1323 K – 72 ks → A. C. + 1273 K – 1080 ks → A.C.	1.173 (serrated)	260
	1473 K – 7.2 ks → W. Q. + 1273 K – 1080 ks → A. C.	1.117 (straight)	255

W.Q.: water-quenched; A.C.: air-cooled; F.C.: furnace-cooled.

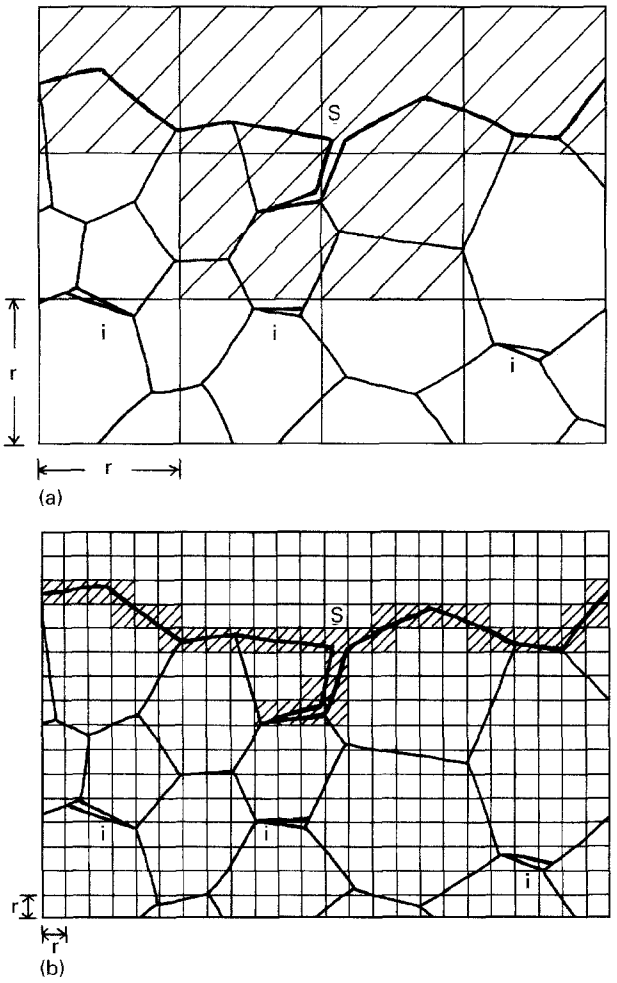

Figure 1 The schematic illustration of the box-counting method applied to the estimation of the fractal dimension of the grain boundary fracture (D_f) in both scale ranges of the fractal analysis (r) larger than ((a)) and smaller ((b)) about one grain boundary length ($n = 6$ in (a) and $n = 32$ in (b), where n is the number of square boxes intersecting the fracture surface or involving the grain boundary cracks linked to the fracture surface (s), and the isolated cracks (i) are not taken into account in this study).

where n_0 and L_0 are constant. Therefore, one can obtain the following equation from Equation 2:

$$\log_{10}L = \log_{10}L_0 + (1 - D_f)\log_{10}r \quad (3)$$

The value of D_f was obtained by regression analysis by the fitting of experimental data to Equation 3.

3. Results and discussion

3.1. Fractal dimension of the grain boundary fracture and microstructures of the ruptured specimens

Fig. 2 shows the relationship between the length of the fracture surface profile (L) and the scale length of the fractal analysis (r) in the specimens of the HS–21 alloy ruptured under a stress of 108 MPa at 1089 K. The datum points were fitted by regression analysis to separate lines for both specimens (Fig. 2a). The original datum points obtained in the scale range smaller than about one grain boundary length ($5.2 \times 10^{-3} \leqslant r/d_g \leqslant 0.52$, d_g: grain diameter) (Fig. 2b) are shifted upward to meet the datum points obtained in the scale range larger than about one grain boundary length ($0.68 \leqslant r/d_g \leqslant 34$) at the intermediate scale length of $r \sim 8 \times 10^{-5}$ m ($r/d_g = 0.60$) in Fig. 2a. The fractal dimension of the grain boundary fracture (D_f) is larger in the specimen with serrated grain boundaries than in the one with straight grain boundaries under the same creep condition. The value of D_f is 1.114 in the smaller scale range of the analysis ($r/d_g \leqslant 0.52$) and 1.208 in the larger scale range ($r/d_g \geqslant 0.68$) in the specimen with straight grain boundaries, whilst the value of D_f in the smaller scale range of the analysis, 1.242, is coincidentally almost the same as the one in the larger scale range, 1.245, in the specimen with serrated grain boundaries.

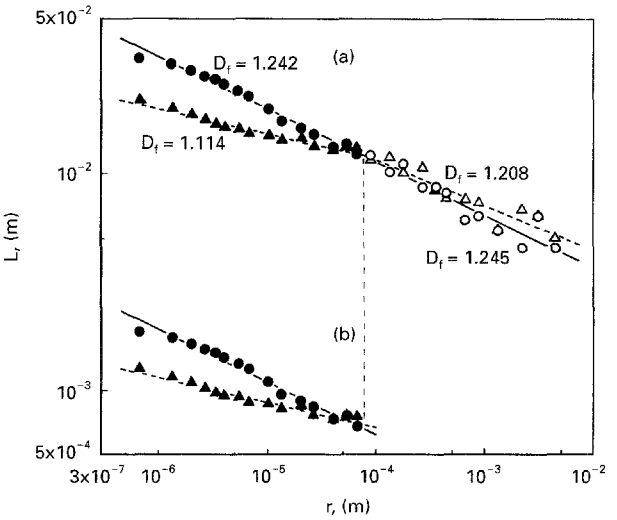

Figure 2 The relationship between the length of the fracture surface profile (L) and the scale of the analysis (r) in the specimens of the HS–21 alloy ruptured under a stress of 108 MPa at 1089 K (D_f is the fractal dimension of the grain boundary fracture, (a) shows the unified results and (b) shows the original datum points obtained in the scale range smaller than about one grain boundary length ($5.2 \times 10^{-3} \leqslant r/d_g \leqslant 0.52$), ○ and ● are serrated grain boundaries, and △ and ▲ are straight grain boundaries).

Table III shows all the results of the fractal analyses in the cobalt-based alloys in this study. As described in section 2, the value of D_f estimated in the scale range (r) larger than about one grain boundary length ($0.68 \leqslant r/d_g \leqslant 34$ for the HS–21 alloy and $0.42 \leqslant r/d_g \leqslant 17$ for the L–605 alloy) was defined for the whole fracture surface profile involving the grain boundary microcracks linked to the fracture surface, while the value of D_f obtained in the scale range smaller than about one grain boundary length ($2.2 \times 10^{-3} \leqslant r/d_g \leqslant 0.65$ for the HS–21 alloy and $1.1 \times 10^{-3} \leqslant r/d_g \leqslant 0.32$ for the L–605 alloy) was defined for the fracture surface profile of five to eight grain boundary lengths involving at least one grain boundary microcrack linked to the fracture surface. In the HS–21 alloy, the value of D_f is larger in the specimen with serrated grain boundaries than in the one with straight grain boundaries in both scale ranges, but the difference in the value of D_f between these specimens is small in the larger scale range ($r/d_g \geqslant 0.68$). In the L–605 alloy, however, there is little difference in the value of D_f between the specimen with serrated grain boundaries and the one with straight grain boundaries in both scale ranges, probably because there is only a small difference in the

TABLE III The fractal dimension of the grain boundary fracture (D_f) and the scale range of the fractal analysis (r) in the ruptured specimens of the cobalt-based alloys.

Alloys	Creep conditions (K)	(MPa)	Grain boundary configuration	Fractal dimension of the grain boundary fracture, D_f (scale range of the fractal analysis (r), m)	
	1089	176	serrated	$1.219\ (6.98\times10^{-7}\sim6.98\times10^{-5})$	$1.173\ (8.88\times10^{-5}\sim3.33\times10^{-3})$
			straight	$1.121\ (6.98\times10^{-7}\sim6.98\times10^{-5})$	$1.148\ (8.88\times10^{-5}\sim3.33\times10^{-3})$
		137	serrated	$1.222\ (5.62\times10^{-7}\sim6.74\times10^{-5})$	$1.226\ (8.90\times10^{-5}\sim4.45\times10^{-3})$
			straight	$1.142\ (5.62\times10^{-7}\sim6.74\times10^{-5})$	$1.208\ (8.90\times10^{-5}\sim4.45\times10^{-3})$
		108	serrated	$1.242\ (6.73\times10^{-7}\sim6.73\times10^{-5})$	$1.245\ (8.90\times10^{-5}\sim4.45\times10^{-3})$
			straight	$1.114\ (6.73\times10^{-7}\sim6.73\times10^{-5})$	$1.209\ (8.90\times10^{-5}\sim4.45\times10^{-3})$
	1200	108	serrated	$1.248\ (6.73\times10^{-7}\sim6.73\times10^{-5})$	$1.235\ (8.90\times10^{-5}\sim4.45\times10^{-3})$
			straight	$1.149\ (6.73\times10^{-7}\sim6.73\times10^{-5})$	$1.211\ (8.90\times10^{-5}\sim4.45\times10^{-3})$
HS–21		78.4	serrated	$1.205\ (6.73\times10^{-7}\sim6.73\times10^{-5})$	$1.239\ (8.90\times10^{-5}\sim4.45\times10^{-3})$
			straight	$1.139\ (6.73\times10^{-7}\sim6.73\times10^{-5})$	$1.221\ (8.90\times10^{-5}\sim4.45\times10^{-3})$
	1255	108	serrated	$1.218\ (6.73\times10^{-7}\sim6.73\times10^{-5})$	$1.252\ (8.82\times10^{-5}\sim4.41\times10^{-3})$
			straight	$1.143\ (6.73\times10^{-7}\sim6.73\times10^{-5})$	$1.187\ (8.82\times10^{-5}\sim3.86\times10^{-3})$
	1311	49.0	serrated	$1.227\ (6.73\times10^{-7}\sim6.73\times10^{-5})$	$1.262\ (8.90\times10^{-5}\sim4.45\times10^{-3})$
			straight	$1.141\ (6.73\times10^{-7}\sim6.73\times10^{-5})$	$1.241\ (8.90\times10^{-5}\sim4.45\times10^{-3})$
		29.4	serrated	$1.227\ (2.81\times10^{-7}\sim8.42\times10^{-5})$	$1.391\ (1.09\times10^{-4}\sim4.38\times10^{-3})$
			straight	$1.117\ (2.81\times10^{-7}\sim8.42\times10^{-5})$	$1.338\ (1.09\times10^{-4}\sim4.38\times10^{-3})$
	1422	19.6	serrated	$1.137\ (5.62\times10^{-7}\sim6.74\times10^{-5})$	$1.349\ (8.90\times10^{-5}\sim4.45\times10^{-3})$
			straight	$1.136\ (5.62\times10^{-7}\sim6.74\times10^{-5})$	$1.376\ (8.90\times10^{-5}\sim4.45\times10^{-3})$
	1089	176	serrated	$1.181\ (6.73\times10^{-7}\sim8.08\times10^{-5})$	$1.186\ (1.10\times10^{-4}\sim4.41\times10^{-3})$
			straight	$1.137\ (6.73\times10^{-7}\sim8.08\times10^{-5})$	$1.147\ (1.10\times10^{-4}\sim4.41\times10^{-3})$
		137	serrated	$1.170\ (2.81\times10^{-7}\sim8.42\times10^{-5})$	$1.225\ (1.09\times10^{-4}\sim3.28\times10^{-3})$
			straight	$1.151\ (2.81\times10^{-7}\sim8.42\times10^{-5})$	$1.225\ (1.34\times10^{-4}\sim3.56\times10^{-3})$
L–605		118	serrated	$1.187\ (6.98\times10^{-7}\sim8.38\times10^{-5})$	$1.229\ (1.11\times10^{-4}\sim3.89\times10^{-3})$
			staight	$1.181\ (6.98\times10^{-7}\sim8.38\times10^{-5})$	$1.246\ (1.11\times10^{-4}\sim3.89\times10^{-3})$
	1311	49.0	serrated	$1.169\ (6.73\times10^{-7}\sim8.08\times10^{-5})$	$1.242\ (1.10\times10^{-4}\sim4.41\times10^{-3})$
			straight	$1.186\ (6.73\times10^{-7}\sim8.08\times10^{-5})$	$1.235\ (1.10\times10^{-4}\sim4.41\times10^{-3})$
		29.4	serrated	$1.158\ (6.73\times10^{-7}\sim8.08\times10^{-5})$	$1.281\ (1.10\times10^{-4}\sim4.41\times10^{-3})$
			straight	$1.157\ (6.73\times10^{-7}\sim8.08\times10^{-5})$	$1.310\ (1.10\times10^{-4}\sim4.41\times10^{-3})$

fractal dimension of the grain boundaries (D_{gb}) between these specimens (1.173 for serrated grain boundaries and 1.117 for straight ones) (Table II). As described in section 2, the stress values show in Table III is the initial creep stress. The value of D_f increases with decreasing creep stress in the larger analysis scale range in these alloys.

Fig. 3 shows the fracture surface profiles and fracture surfaces of the specimens of the HS–21 alloy ruptured under a stress of 108 MPa at 1089 K. The tensile direction is parallel to the vertical in the photograph. The number of grain boundary microcracks linked to the fracture surface seems to be larger in the specimens with serrated grain boundaries (Fig. 3a) than in the one with straight grain boundaries (Fig. 3b). The fracture surface profiles of these specimens are different from each other at higher magnification (Fig. 3(c, d)). Many large precipitates were also observed on the serrated grain boundaries (for example, indicated by arrows in Fig. 3c). The fracture surface of the specimen with serrated grain boundaries consists of steps and ledges with small dimples corresponding to serrated grain boundaries (Fig. 3e), while that of the specimen with straight grain boundaries is typical of grain boundary facets (Fig. 3f) [16]. Thus, these differences in the number of grain boundary microcracks and in the fracture appearance lead to the differences in the value of D_f (Table III). As shown in the caption of Fig. 3, the specimen with serrated grain boundaries generally has the longer rupture life and the larger creep ductility than the one with straight grain boundaries [16–18]. Serrated grain boundaries are generally effective in retarding grain boundary sliding which leads to the initiation and growth of grain boundary microcracks (19, 20), although a larger number of grain boundary microcracks was observed in the specimen with serrated grain boundaries (Fig. 3a). The details are described in the next section (3.2). Oxidation during high-temperature creep may also affect grain boundary miccrocracking [21], but the effect of oxidation on grain boundary fracture is unclear in the cobalt-based alloys used in this study.

Fig. 4 shows the fracture surface profiles of the specimens of the L–605 alloy ruptured under a stress of 118 MPa at 1089 K. The tensile direction is parallel to the vertical in the photographs. There is little difference in the number of grain boundary microcracks linked to the fracture surface (Fig. 4(a, b)) or in the fracture surface profile (Fig. 4(c, d)) between the specimen with serrated grain boundaries and the one with straight grain boundaries, since there is no obvious difference in the microstructure between these specimens. The rupture life of the specimen with serrated grain boundaries is almost the same as that of the specimen with straight grain boundaries in the L–605 alloy under this creep condition (as is shown in the figure caption). The fracture surfaces of both

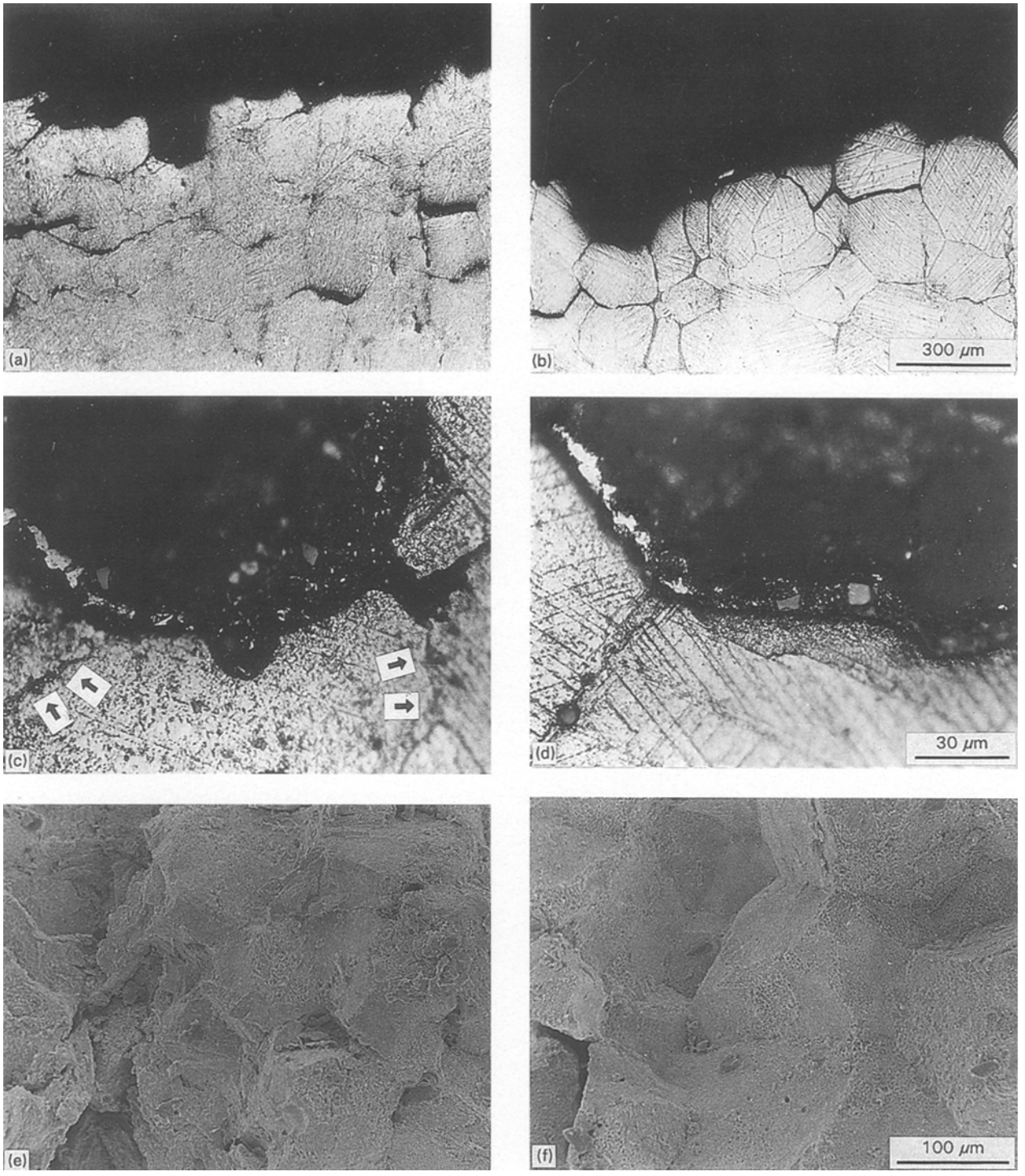

Figure 3 Fracture surface profiles and fracture surfaces in the specimens of the HS–21 alloy ruptured under a stress of 108 MPa at 1089 K. (a), (c) and (e) are serrated grain boundaries (t_r = 848 ksec, ε_r = 0.0503) and (b), d) and (f) are straight grain boundaries (t_r = 526 ksec, ε_r = 0.0254) (t_r: rupture life; ε_r: elongation).

specimens were ductile ones with small dimples [18]. Therefore, the value of D_f in the specimen with serrated grain boundaries is almost the same as that in the specimen with straight grain boundaries in the L–605 alloy (Table III).

3.2. Fractal dimension of the grain boundary fracture in the larger scale range

Fig. 5 shows the relationship between the fractal dimension of the grain boundary fracture (D_f) estimated in the scale range of the analysis larger than about one grain boundary length ($0.68 \leqslant r/d_g \leqslant 34$) and the creep stress in the ruptured specimens of the HS–21 alloy. The value of D_f increases from about 1.1 to 1.4 with decreasing creep stress in this scale range in the temperature range from 1089–1422 K. The value of D_f for the specimen with serrated grain boundaries is generally a little larger than that of the specimen with straight grain boundaries. Fig. 6 shows the relationship between the fractal dimension of the grain boundary fracture (D_f) estimated in the scale range larger than about one grain boundary length

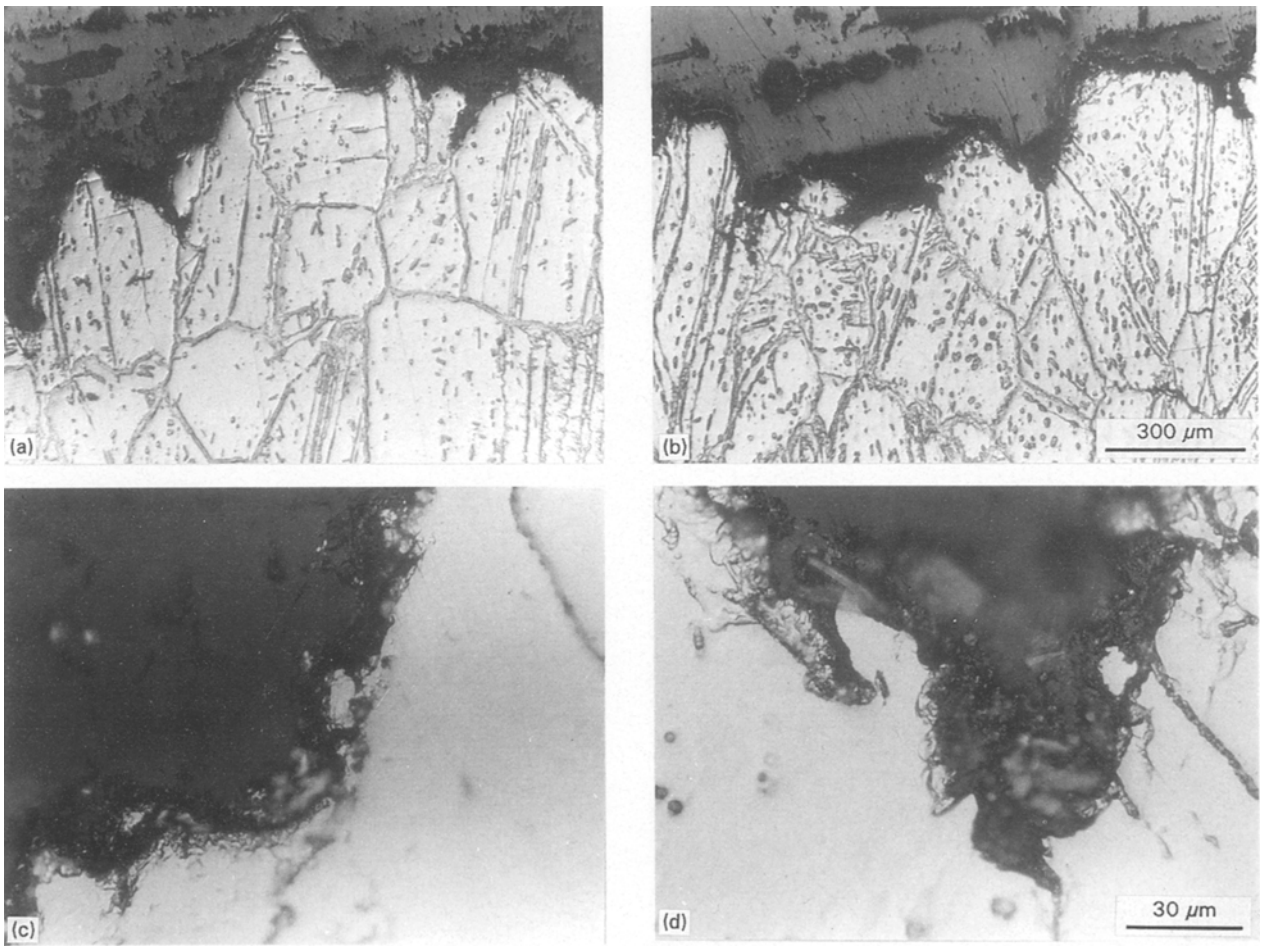

Figure 4 Fracture surface profiles in the specimens of the L–605 alloy ruptured under a stress of 118 MPa at 1089 K. (a) and (c) are serrated grain boundaries ($t_r = 1740$ ksec, $\varepsilon_r = 0.214$) and (b) and (d) are straight grain boundaries ($t_r = 1810$ ksec, $\varepsilon_r = 0.231$) (t_r: rupture life; ε_r: elongation).

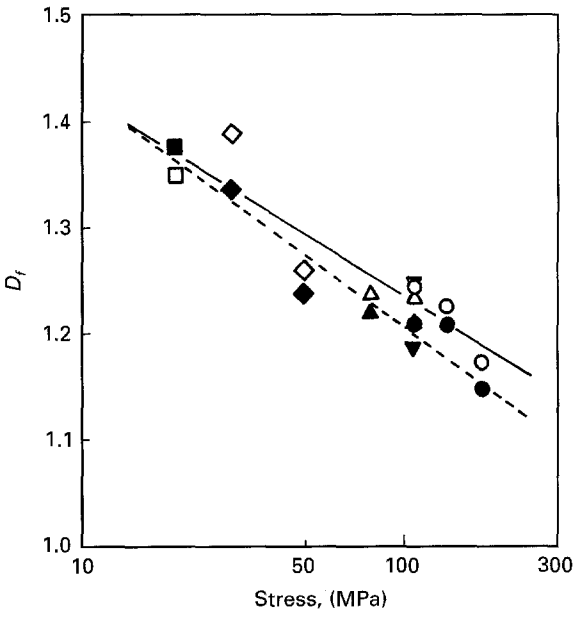

Figure 5 The relationship between the fractal dimension of the grain boundary fracture (D_f) estimated in the scale range of the analysis (r) larger than about one grain boundary length ($0.68 \leqslant r/d_g \leqslant 34$) and creep stress in the ruptured specimen of the HS–21 alloy. Data taken for the serrated grain boundary at; (○) 1089 K, (△) 1200 K, (▽) 1255 K, (◇) 1311 K and (□) 1422 K. The data are linked by the (—) line. Data taken for the straight grain boundary are represented by; (●) 1089 K, (▲) 1200 K, (▼) 1255 K, (◆) 1311 K and (●) 1422 K and are linked by the dashed (– – –) line.

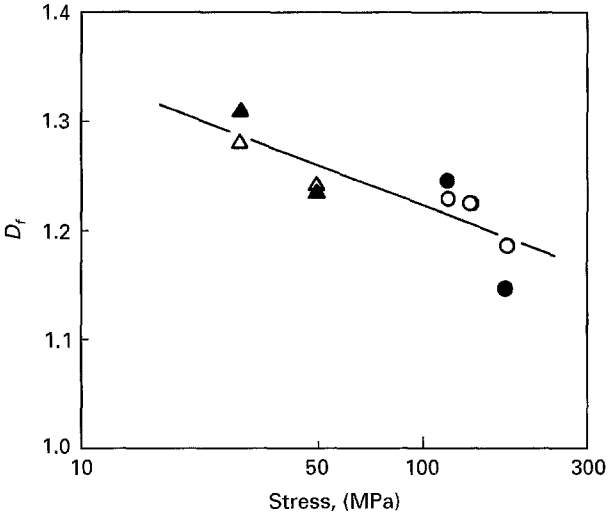

Figure 6 The relationship between the fractal dimension of the grain boundary fracture (D_f) estimated in the scale range of the analysis (r) larger than about one grain boundary length ($0.42 \leqslant r/d_g \leqslant 17$) and creep stress in the ruptured specimens of the L–605 alloy. Data taken for the serrated grain boundary at; (○) 1089 K, (△) 1311 K and for the straight grain boundary at (●) 1089 K and (▲) 1311 K.

($0.42 \leqslant r/d_g \leqslant 17$) and the creep stress in the ruptured specimens of the L–605 alloy. The value of D_f also increases with decreasing creep stress in this alloy, but the stress dependence of D_f is a little smaller in the

L–605 alloy than in the HS–21 alloy. There is only a slight difference in the value of D_f between specimens with serrated grain boundaries and those with straight grain boundaries in the L–605 alloy, and all datum points can be fitted to a single line (Fig. 6).

Gokhale *et al.* [22] reported that if the anisotropy of the fracture surface is rotationally symmetric with respect to the vertical axis in the vertical section method, then all the vertical section fracture profiles are expected to be statistically similar, and the fractal dimension of a fracture surface estimated on any one vertical section profile should yield a reliable value in such a case. The grain boundary fracture surface examined in this study are considered to be rotationally symmetric with respect to the vertical axis, since the intersection of the grain boundary microcracks with the fracture surface (the number of the observed microcracks) is related to the distance from the specimen surface where a lot of these microcracks exist. For the above reasons, the fractal dimension of the grain boundary fracture surface profile (the fractal dimension of the grain boundary fracture, D_f) estimated from a single vertical section involving the vertical axis is considered to yield a reliable value in the scale range larger than about one grain boundary length in this study.

Gokhale *et al.* [22] found that fracture surfaces of isotropic materials (having isotropic microstructures as well) generated by a uniaxial stress are expected to be rotationally symmetric with respect to the stress (vertical) axis. Drury and Gokhale [23] also pointed out the importance of the number of samples required for minimizing the statistical sampling error in the fractal analysis. As for the value of D_f estimated in the scale range smaller than about one grain boundary length, the number of samples taken (five to eight grain boundaries) in the present analysis is considered to give a reliable value of D_f, since the micro-structures of the grain boundary fracture surfaces seem to be isotropic (uniform) in the ruptured specimens of the cobalt-based alloys (Fig. 3(e, f)). As will be described in the next section (3.3), the values of D_f estimated in this scale range have a small standard deviation in the same kind of specimens, and is essentially independent of the creep conditions.

As is described in section 2, the grain boundary microcracks linked to the fracture surface are also included by the box-counting method applied to the estimation of the value of D_f in this study. Fig. 7 shows the relationship between the number of grain boundary microcracks per unit projected length of the fracture surface profile (N) and the creep stress in the ruptured specimens of the HS–21 alloy. The stress dependence of the number of the grain boundary microcracks resembles that of the value of D_f (Fig. 5). The value of N increases with decreasing creep stress in specimens with either serrated grain boundaries or with straight grain boundaries. The value of N was larger in the specimen with serrated grain boundaries than in the one with straight grain boundaries.

Ashby [24], Ashby, Raj and Gifkins [25], Raj and Ashby [26], and Crossman and Ashby [27] have discussed the effects of grain size and grain boundary

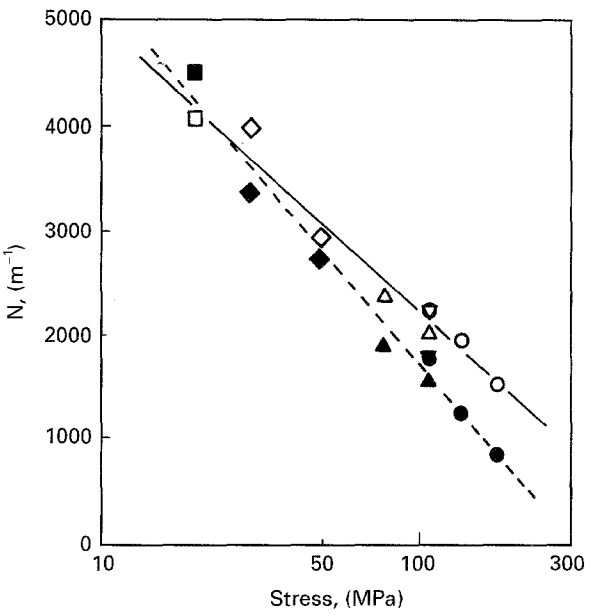

Figure 7 The relationship betweeen the number of grain boundary microcracks linked to the fracture surface per unit length of the fracture surface profile (N) and creep stress in the ruptured specimens of the HS–21 alloy. Data taken for the serrated grain boundary at; (○) 1089 K, (△) 1200 K, (▽) 1255 K, (◇) 1311 K (□) 1422 K and the data are linked by the continuous line. Data was taken for the straight grain boundary at; (●) 1089 K, (▲) 1200 K, (▼) 1255 K, (◆) 1311 K and (■) 1422 K the data are linked by the dashed (– – –) line.

structure on the deformation mechanisms. According to their results [24–27], the grain boundary ledges, bumps and curvature as well as grain boundary precipitates raise grain boundary viscosity and make grain boundary sliding difficult in the regime where creep strain depends on grain boundary sliding. This is the reason why serrated grain boundaries are effective in retarding the grain boundary sliding. However, at the same time, grain boundary sliding causes tensile stress concentration at grain boundary ledges, bumps, precipitates or triple junctions, which results in the formation of grain boundary microcracks or wedge-shaped cracks [25–27]. This may lead to a larger number of grain boundary microcracks in specimens with serrated grain boundaries. The relative amount of grain boundary sliding to total creep deformation is larger under lower stresses and high temperatures in the regime where creep strain depends on grain boundary sliding [27–29]. This implies that the number of grain boundary microcracks is larger under lower stresses in both specimens with serrated grain boundaries and those with straight grain boundaries. However, the crack growth rate was lower in specimens with serrated grain boundaries [30, 31], because the large precipitates on the serrated grain boundaries may impede crack growth (Fig. 3c).

A similar but weaker stress dependence of the number of grain boundary microcracks linked to the fracture surface is also observed in the L–605 alloy, as is shown in Fig. 8. All the datum points are fitted to a single line in this alloy, since there is almost no difference in the micro-structure between the specimens with serrated grain boundaries and those with straight grain boundaries (Fig. 4). Thus, the value of

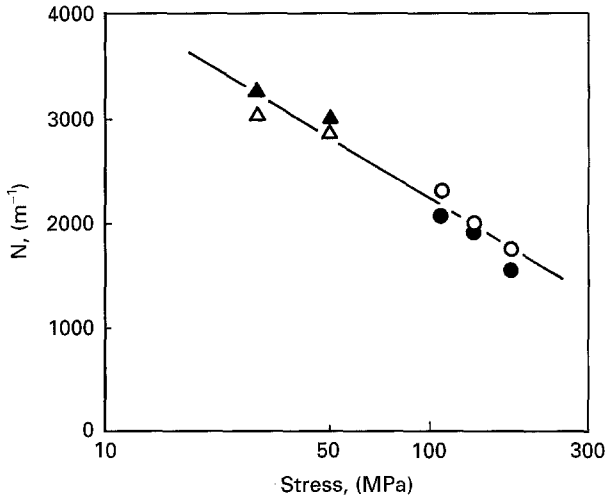

Figure 8 The relationship between the number of grain boundary microcracks linked to the fracture surface per unit length of the fracture surface profile (N) and creep stress in the ruptured specimens of the L–605 alloy. Data taken for the serrated grain boundary at; (○) 1089 K, (△) 1311 K. Data taken for the straight grain boundary at (◆) 1089 K and (▲) 1311 K.

D_f estimated in the scale range larger than about one grain boundary length depends not only on the microstructure (grain boundary configuration) but also on the number of grain boundary microcracks linked to the fracture surface (creep conditions) in the cobalt-based alloys.

3.3. Fractal dimension of the grain boundary fracture in the smaller scale range

Fig. 9 shows the relationship between the fractal dimension of the grain boundary fracture (D_f) estimated in the scale range of the analysis (r) smaller than about one grain boundary length ($2.2 \times 10^{-3} \leqslant r/d_g \leqslant 0.65$ for the HS–21 alloy and $1.1 \times 10^{-3} \leqslant r/d_g \leqslant 0.32$ for the L–605 alloy) in the ruptured specimens of the cobalt-based superalloys. The value of D_f gives a stress–independent constant value except in the specimen with serrated grain boundaries ruptured at 1422 K, in which severe oxidation and surface diffusion of atoms during creep may have affected the configuration of the fracture surface profile [20]. In the HS–21 alloy, the averaged value and the standard deviation of D_f were respectively 1.226 and 0.0136 for the specimens with serrated grain boundaries, while the averaged value and the standard deviation of D_f were respectively 1.133 and 0.0127 for those with straight grain boundaries. As described in the previous sections (sections 2 and 3.2), only one vertical section involving the vertical axis was examined for the estimation of the value of D_f in each specimen, and the fracture surface profile of five to eight grain boundary lengths was analysed in the scale range smaller than about one grain boundary length. There is a statistically significant difference in the value of D_f between the specimens with serrated grain boundaries and those with straight grain boundaries in the HS–21 alloy, as indicated by those averaged values and the small standard deviation

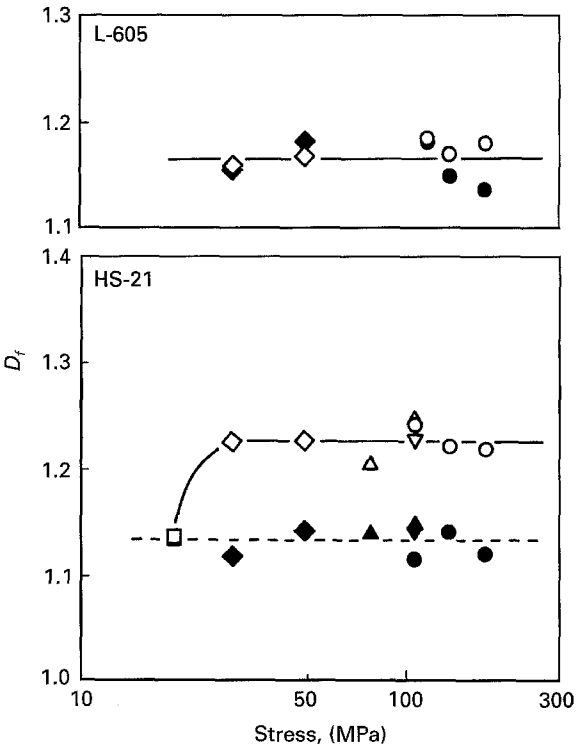

Figure 9 The relationship between the fractal dimension of the grain boundary fracture (D_f) estimated in the scale range of the anlysis (r) smaller than about one grain boundary length ($2.2 \times 10^{-3} \leqslant r/d_g \leqslant 0.65$ for the HS–21 alloy and $1.1 \times 10^{-3} \leqslant r/d_g \leqslant 0.32$ for the L–605 alloy) and creep stress in the ruptured specimens of the cobalt-based alloys. For the L–605 alloy data was taken on the serrated grain boundary at; (○) 1089 K and (◇) 1311 K and on the straight grain boundary at (●) 1089 K (▲) 1311 K. For the HS-21 alloy data were taken on the serrated grain boundary at, (○) 1089 K, (△) 1200, (▽) 1255 K, (◇) 1311 K and (□) 1422 K. Data was also taken on the straight grain boundary at; (●) 1089 K, (▲) 1200 K, (▼) 1255 K, (◆) 1311 K and (■) 1422 K.

of D_f. The averaged value and the standard deviation of D_f were respectively 1.167 and 0.0166 for all the specimens in the L–605 alloy. Thus, it is concluded that reliable value of D_f were also obtained in the scale range smaller than about one grain boundary length on the ruptured specimens of the cobalt-based alloys used in this study. In general, the changes in the value of D_f can be derived not only from the statistical variation in the fracture surface profiles but also from the local variation in the microstructure or in the fracture mechanisms [22, 23]. Therefore, the significance of the changes in the value D_f should be carefully examined by taking these variations into account.

As for the temperature dependence of the value of D_f, the relative contribution of grain boundary sliding to creep strain generally increases with a rise in temperature [27–29], and this may lead to an increased number of grain boundary microcracks which result in an increase in the value of D_f estimated in the scale range larger than about one grain boundary length. However, the temperature dependence of D_f is not clear in this study, since there are only a few available datum points for D_f taken under the constant initial stress at different temperatures.

4. Conclusions

The effects of grain boundary configuration and creep conditions on the fractal dimension of the grain boundary fracture surface profile (the fractal dimension of the grain boundary fracture, D_f) were investigated using cobalt-based heat resistant alloys, namely, HS–21 and L–605 alloys. Creep–rupture experiments were carried out under initial creep stresses of 19.6–176 MPa in the temperature range from 1089–1422 K in air. The results obtained are summarized as follows.

(1) The fractal dimension of the grain boundary fracture, D_f, was larger in specimens with serrated grain boundaries than in those with straight grain boundaries in the HS–21 alloy under the same creep condition. The difference in the value of D_f between these specimens was relatively small in the scale range of the fractal analysis (r) larger than about one grain boundary length ($0.68 \leqslant r/d_g \leqslant 34$, where d_g is the grain diameter). The value of D_f of the specimen with serrated grain boundaries was almost the same as that of the specimen with straight grain boundaries in the L–605 alloy. This is thought to be due to the fact that there was no obvious differences in the microstructures of these specimens.

(2) The value of D_f increased from about 1.1 to 1.4 with decreasing creep stress in the scale range of the analysis (larger than about one grain boundary length ($0.68 \leqslant r/d_g \leqslant 34$ for the HS–21 alloy and $0.42 \leqslant r/d_g \leqslant 17$ for L–605 alloy) in both alloys in the temperature range from 1089–1422 K. The stress dependence of D_f was larger in the HS–21 alloy than in the L–605 alloy, and this was explained by the stress dependence of the number of grain boundary microcracks linked to the fracture surface. These experimental results were correlated to the grain boundary configuration of the specimens, and the stress and temperature dependence of grain boundary sliding, which controlled the initiation and growth of the grain boundary microcracks.

(3) The value of D_f exhibited essentially a stress-independent constant value in the scale range of the analysis (smaller than about one grain boundary length ($2.2 \times 10^{-3} \leqslant r/d_g \leqslant 0.65$ for the HS–21 alloy and $1.1 \times 10^{-3} \leqslant r/d_g \leqslant 0.32$ for the L–605 alloy) in both alloys. The averaged value of D_f was larger in specimens with serrated grain boundaries than in those with straight grain boundaries in the HS–21 alloy, whilst the averaged value of the fractal dimension was the same for all the specimens in the L–605 alloy.

References

1. B. B. MANDELBROT, "The Fractal Geometry of Nature," translated by H. Hironaka (Nikkei Science, Tokyo, 1985), p. 25.
2. B. B. MANDELBROT, D. E. PASSOJA and A. J. PAULLAY, *Nature*, **308** (1984) 721.
3. K. BANERJI and E. E. UNDERWOOD, in Proc. 6th Conf. on Fracture, New Delhi, India, 1984, Advances in Fracture Research, eds S. R. VALLURI, D. M. R. TAPLIN, P. RAMA RAO, J. F. KNOTT, R. DUBEY, (Pergamon Press, London, 1984), 1612 p. 1371.
4. E. E. UNDERWOOD and K. BANERJI, *Mater. Sci. Eng.* **80** (1986), 1.
5. E. HORNBOGEN, *Z, Metallkd.* **78** (1987), 622.
6. *Idem. Int. Mater. Rev.* **34** (1989) 277.
7. R. H. DAUSKARDT, F. HAUBENSAK and R. O. RITCHIE, *Acta Metall.* **38** (1990) 142.
8. M. TANAKA and H. IIZUKA, *Z. Metallkd.* **82** (1991) 442.
9. M. TANAKA, *J. Mater. Sci.* **27** (1992) 4717.
10. *Idem. Ibid.* **28** (1993) 5753.
11. *Idem. Z. Metallkd.* 84 (1993) 697.
12. H. TAKAYASU, "Fractals in the Physical Sciences," (Manchester University Press, Manchester, 1990), p. 6.
13. S. ISHIMURA and S. ISHIMURA, "Fractal Mathematics," (Tokyo Tosho Co., Tokyo, 1990), p. 246.
14. C. S. PANDE, L. E. RICHARDS, N. LOUAT, B. D. DEMPSEY and A. J. SCHWOEBLE, *Acta Metall.* **35** (1987) 1633.
15. K. BANERJI, *Metall. Trans. A*, **19A** (1988) 961.
16. M. TANAKA, O. MIYAGAWA, T. SAKAKI and D. FUJISHIRO, *J. Iron Steel Inst. Japan* **65** (1979) 939.
17. M. TANAKA, H. IIZUKA and F. ASHIHARA, *J. Mater. Sci.* **24** (1989) 1623.
18. M. TANAKA, H. IIZUKA and M. TAGAMI, *ibid.* **24** (1989) 2428.
19. M. TANAKA, O. MIYAGAWA, T. SAKAKI, H. IIZUKA and D. FUJISHIRO, *Ibid.* **23** (1988) 621.
20. M. TANAKA, H. IIZUKA and F. ASHIHARA, *Ibid.* **27** (1992) 2636.
21. R. OHTANI and S. NAKAYAMA, *J. Mater. Sci. Japan* **32** (1983) 635.
22. A. M. GOKHALE, W. J. DRURY and S. MISHRA, in ASTM STP1203, American Society for Testing and Materials, Philadelphia, (1993), p. 3.
23. W. J. DRURY and A. M. GOKHALE, *ibid.* p. 58.
24. M. F. ASHBY, *Acta Metall.* **20** (1972) 887.
25. M. F. ASHBY, R. RAJ and R. C. GIFKINS, *Scripta Metall.* **4** (1970) 737.
26. R. RAJ and M. F. ASHBY, *Metall. Trans.* **2** (1971) 1113.
27. F. W. CROSSMAN and M. F. ASHBY, *Acta Metall*, **23** (1975) 425.
28. F. GAROFALO, "Fundamentals of Creep and Creep Rupture in Metals," translated by M. ADACHI, (Maruzen Book Co. Ltd., Tokyo, 1968). p. 124.
29. T. G. LANGDON and R. B. VASTAVA, in ASTM STP 765, American Society for Testing and Materials, Philadelphia, (1982), p. 435.
30. M. TANAKA, H. IIZUKA and F. ASHIHARA, *J. Mater. Sci.* **23** (1988) 3827.
31. M. TANAKA and H. IIZUKA *Trans. ASME, J. Mater. Sci. Technol.* **112** (1990), 353.

Received 6 March 1995
and accepted 15 December 1995